Journal of Power Sources 380 (2018) 64–75

Contents lists available at ScienceDirect

Journal of Power Sources

journal homepage: www.elsevier.com/locate/jpowsour

Effect of CO_2 absorption on ion and water mobility in an anion exchange membrane

Jing Peng[a,**], Asa L. Roy[b], Steve G. Greenbaum[c], Thomas A. Zawodzinski[a,d,*]

[a] Department of Chemical & Biomolecular Engineering, University of Tennessee, Knoxville, TN 37996, USA
[b] Bredesen Center for Interdisciplinary Research and Education, University of Tennessee, Knoxville, TN 37996, USA
[c] Department of Physics & Astronomy, Hunter College of the City University of New York, New York, NY 10065, USA
[d] Physical Chemistry of Materials Group, Oak Ridge National Laboratory, Oak Ridge, TN 37831, USA

HIGHLIGHTS

- An anion exchange membrane Tokuyama A201 was studied in OH^-, Cl^- and HCO_3^- forms.
- Water uptake, density, ionic conductivity and water transport of AMEs was reported.
- The effect of CO_2 absorption in the water uptake and conductivity of AEM was observed.
- Water and HCO_3^- ion diffusivity was characterized by PFG-NMR technique.
- The applicability of Nernst-Einstein equation in AEM was discussed.

GRAPHICAL ABSTRACT

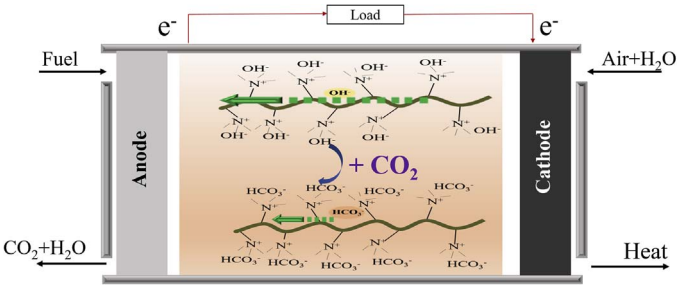

ARTICLE INFO

Keywords:
Anion exchange membrane
Ion mobility
Water transport
Carbon dioxide adsorption
Fuel cell
Nernst-Einstein equation

ABSTRACT

We report the measured water uptake, density, ionic conductivity and water transport properties in Tokuyama A201 membrane in OH^-, HCO_3^- and Cl^- forms. The water uptake of the AEM varies with anion type in the order $\lambda(OH^-) > \lambda(HCO_3^-) > \lambda(Cl^-)$ for samples equilibrated with the same water vapor activity (a_w). The conductivity of the AEM is reduced by absorption of CO_2. Pulsed-field gradient nuclear magnetic resonance (PFG-NMR) measurements were utilized to characterize the diffusivity of water and HCO_3^- ion. The anion diffusion coefficient and membrane conductivity are used to probe the applicability of the Nernst-Einstein equation in these AEMs.

1. Introduction

Sustained work on low temperature proton exchange membrane fuel cells (PEMFCs) for transportation and portable applications over the past several decades has significantly lowered the projected costs of fuel cell stacks for electric vehicles. Driven in part by the effort to reduce costs, anion exchange membrane fuel cells (AEMFCs) have received increased interest in recent years. AEMFCs differ from PEMFCs by the ion that is exchanged through the membrane, hydroxide ions rather than protons. Thus AEMFCs operate in a basic environment in the cell. There are more promising non-precious metal oxygen reduction catalysts for basic environments than acidic ones, making it possible to substitute for the expensive platinum-based cathode catalysts in PEMFCs with relatively common, cheap materials in AMEFCs [1–3]. Due to the possible utilization of non-precious metal catalysts, AEMFCs are also claimed to be more tolerant to fuel crossover [4].

* Corresponding author. 1512 Middle Drive, Knoxville, TN 37996-2200, USA.
** Corresponding author.
E-mail addresses: jpeng9@utk.edu (J. Peng), tzawodzi@utk.edu (T.A. Zawodzinski).

https://doi.org/10.1016/j.jpowsour.2018.01.071
Received 17 November 2017; Received in revised form 19 January 2018; Accepted 23 January 2018

In AEMFCs an anion exchange membrane (AEM) is used as a polymer electrolyte allowing transport of the charge carriers and water and perhaps some other species between the two electrodes. As for any membrane, an ideal AEM should have high ionic conductivity, good mechanical and thermal stability, good durability, and low cost [2]. Recently, there have been a number of encouraging reports on AEMs [5–8]. However, the development of the AEM and its deployment in the fuel cell still face several significant challenges. AEMs based on hydrocarbon backbones and functionalized with quaternary ammonium groups typically have lower ionic conductivity than the PEM counterparts, often with poor mechanical and thermal stability [1,9]. To some extent, this reflects the immature state of the field. Unlike the case for proton exchange membranes (PEMs), for which Nafion® and a number of related perfluorinated sulfonic acid (PFSAs) were available from the earliest stages of device development, there is no manufacturer of AEMs suitable for AEMFCs. Thus, the available membranes are often experimental in nature and as such are not processed to yield sufficient mechanical and thermal properties. An exception to this, until recently, has been the A201 membranes of Tokuyama.

The emphasis in the literatures on AEMs has tended heavily toward probing their chemical stability such as the chemical degradation of AEM in alkaline media due to an attack of OH^- on AEM, causing the decreasing of ionic conductivity [10–12], while the transport properties receive somewhat less interest beyond reports of conductivity. Transport in AEMFCs is significantly more complicated than in PEMFCs. Water is both a product and a reactant in AEMFCs while it is a product in PEMFCs. Therefore, understanding how to properly maintain a water balance that avoids flooding the electrodes and drying out the membrane requires a greater understanding of the water transport properties in AEMs. Their importance for optimizing the cell performance of AEMFCs has been discussed by Omasta et al. [13] and Gottesfeld et al. [14].

Furthermore, hydroxide-form AEMs tend to take in carbon dioxide from the air, complicating the understanding of transport properties in AEMFCs due to the formation of HCO_3^- and CO_3^{2-} ions resulting from reaction of the OH^- in the membrane with carbon dioxide [15]. There has been some work conducted to study the effect of uptake of CO_2 on the AEM using different methods. The ionic conductivity of OH^- and CO_3^{2-}/HCO_3^- has been reported for some AEMs [16] and the uptake of CO_2 to form bicarbonate has a deleterious effect, lowering conductivity. However, the effect of CO_2 absorption on the uptake of water and other transport-related properties has been less studied. Among the few reports of transport properties of AEMs, water flux measurements were performed to study the water transport in AEM, then used to predict the ion diffusion coefficient in the AEM based on kinetic theory [17]. Another important method for transport study is Pulsed Field Gradient (PFG) Nuclear Magnetic Resonance (NMR), which has been used for measuring the diffusivity of water, methanol and OH^- in some AEMs [18–21].

Analogous to the protons in the proton exchange membranes (PEMs), the transport of hydroxide ion in AEM is expected to occur through three dominant mechanisms: the 'Grotthuss' mechanism (or structural diffusion), diffusion and convection [22–25]. At high water content, the most important transport mechanism of OH^- ions occurs via structural diffusion of 'defects' (H-vacancies) through the hydrogen bond network formed by charged ions and water, with lower mobility compared to proton [26]. In aqueous solutions, the transport coefficient $D_{OH^-} = 5.3 \times 10^{-9}\,m^2/s$ is smaller than $D_{H^+} = 9.3 \times 10^{-9}\,m^2/s$ at 25 °C [27]. There is a larger difference in mobility of protons and hydroxide ions in polymer membranes than that observed in liquid water. Varcoe et al. [28] reported a systematic study of the conductivity of poly(tetrafluoroethylene-co-hexafluoropropylene) (FEP)-grafted-poly(vinylbenzyltrimethylammonium) hydroxide AEM and poly(ethylene-co-tetrafluoroethylene) (ETFE)-grafted-poly(vinylbenzyltrimethylammonium) hydroxide AEM at 30 °C. These two AEMs show conductivity of 0.018 and $0.012\,S\,cm^{-1}$ for the samples equilibrated at water vapor activity (a_w) = 1, 30 °C, respectively, which are much lower than $0.078\,S\,cm^{-1}$ of Nafion® 115. Grew and Chiu [29] reported a 'dusty fluid' model for predicting the effect of a_w and membrane properties on the ionic conductivity in AEMs. Nafion® 115 experimental conductivity data successfully validated this model, in which water uptake, ion concentration, and membrane and pore volume fraction are indispensable parameters for evaluating the ionic conductivity. In addition, Grew and Chiu analyzed the OH^- conductivity in ETFE and FEP based AEMs. Unlike the experimentally measured conductance of OH^- in aqueous H_2O which is about 3/5 that of H^+ in aqueous H_2O, the conductivities of ETFE and FEP based AEMs are $0.010\,S\,cm^{-1}$ and $0.014\,S\,cm^{-1}$, respectively, only about 1/7 and 1/4 of that of Nafion® 115 ($0.072\,S\,cm^{-1}$) at 30 °C based on their 'dusty fluid' model. The lower mobility of OH^- relative to H^+ in both aqueous solution and polymer system is due to the different properties of OH^- and H^+: excess H^+ ions are directly moved via exchange in an extended hydrogen bond network and can move without requiring significant activation and/or solvent rearrangement. The solvation of OH^- is more stable, and its motion disturbs the hydrogen bond network [23,30,31]. In the polymer, the coulombic interactions between the OH^- and the functional ammonium group could also contribute to the larger disparity of ion mobility in membranes [32].

Hibbs et al. [19] have reported the transport properties of a series of chloromethylated polysulfone (PS)-AEMs, which are functionalized by quaternary ammonium ions to obtain different IEC values. In Hibbs' work, the water uptake, hydroxide anion conductivity and water self-diffusion coefficient were compared between PS-AEMs with different IECs, sulfonated poly (phenylene) (SDAPP) and Nafion® 115. Generally, the polysulfone based AEMs with higher IECs tend to achieve higher water uptake, hydroxide anion conductivity and water diffusion coefficient. The highest conductivity of AEMs reported in this work is $0.035\,S\,cm^{-1}$ when IEC of PS-AEM is $1.89\,mmol\,g^{-1}$. The water uptake of PS-AEMs equilibrated in liquid water is similar to that of the SDAPP with the same IEC, which may be because polysulfone and polyphenylene backbones have very high T_g values and most likely similar chain stiffness. Nafion® shows slightly higher water uptake than the other two membranes at low IECs. Again, this may be caused by the more flexible aliphatic backbone chain in the Nafion® (compared to aromatic backbones in SDAPP and PS-AEMs). This work also characterized the water diffusion coefficient of fully hydrated PS-AEM, SDAPP membranes with different IECs and Nafion®. The results exhibit a higher water diffusion coefficient in PS-AEM than in SDAPP for a given IEC. Differential scanning calorimetry (DSC) results show a higher enthalpy of melting of water in the PS-AEMs than in SDAPP membranes with similar IECs. The higher water diffusion coefficient and enthalpy of melting of water suggest more free movement of water molecules within the PS-AEMs as compared to SDAPP membranes. However, faster water diffusivity in PS-AEM does not lead to higher conductivity. The ion conductivity and pressure driven water permeability of these PS-AEMs with IECs ranging from 1.04 to $1.89\,mmol\,g^{-1}$ were smaller than those of sulfonated PEMs including SDAPP membranes with similar IECs and Nafion® 115 [19]. Based on the data provided in this paper, the water in the AEM is more mobile than in the sulfonated PEM at comparable water content. However, the ionic conductivity (normalized for the difference in hydroxide and proton ion mobility) and pressure-driven water permeability are not superior in the PS-AEM system. One of the reasons for this may due to the absence of phase separation in the PS-AEM because these membranes were functionalized with cationic groups after casting, while the phase separation in sulfonated PEMs such as SDAPP help to create hydrated transport pathways and promote transport in the membrane. It also is believed a lower degree of OH^--quaternary ammonium dissociation compared to the H^+-sulfonate ion dissociation could be another reason that causes the disparity of transport properties in AEM and PEM.

So far, only a few AEMs have been commercialized to a limited extent as they are typically unstable in alkaline or electrochemical environments [2]. Hydroxide-form Tokuyama A201 has been reported to have a conductivity of $29\,mS\,cm^{-1}$, which is the highest among

commercially prepared AEMs [2]. There are also some highly conductive, non-commercialized AEM reported recently. Pandey et al. [33] reported an e-beam grafted poly(ethylene-co-tetrafluoroethylene) (PTFE) AEM which exhibits a conductivity of 0.132 S cm^{-1} at 80 °C and 0.061 S cm^{-1} at 40 °C, a_w 0.95. Yang et al. [34] synthesized an alkaline nanocomposite polymer electrolyte composed of polyvinyl alcohol (PVA) polymer matrix with nanosized ZrO_2 ceramic fillers, which exhibits a very high ionic conductivity value of 0.267 S cm^{-1} at 20 °C.

Some AEMs have been applied in AEMFCs and achieved excellent performance. The peak power density of AEMFC using quaternary ammonia polysulfone-based AEMs was successfully improved to 1.0 W cm^{-2} from 0.6 W cm^{-2} by replacing the Pt/C catalyst by PtRu/C catalyst in 2015 [35]. A radiation-grafted ETFE-based AEM, functionalized with benchmark benzyltrimethylammonium has been reported by Omasta et al. [13]. This membrane, with conductivity 0.132 S cm^{-1} at a_w 0.95, 80 °C, obtained a peak power density of 1.4 W cm^{-2} at 60 °C in a H_2/O_2 AEMFC. Wang et al. [36] also reported a benzyltrimethylammonium-type AEM, prepared by the radiation grafting of vinylbenzyl chloride onto ETFE film, which achieves Cl^- anion conductivity up to 0.068 S cm^{-1} and a peak power density of 1.16 W cm^{-2} in a H_2/O_2 AEMFC at 80 °C.

The formation of CO_3^{2-} and HCO_3^- ions, which are larger and less mobile than OH^-, lowers the conductivity of the AEM and reduces the cell efficiency [21,37]. The CO_3^{2-} and HCO_3^- formation also will lower the pH of the system. One positive effect is that CO_3^{2-} and HCO_3^- ions are less nucleophilic than OH^-, and the two ions have a lower tendency to attack the cationic sites of AEM [38]. The latter two effects both help to stabilize the membrane and extend the operational lifetime of AEMFCs [38]. At high current density, the CO_3^{2-} and HCO_3^- species are expected to be purged from the membrane through the cathode and released out of the fuel cell with excess fuel in the anode to a certain extent, the 'self-purging' mechanism. In addition to transport in the AEM, the presence of CO_2 also influences the electrochemical kinetics of the two electrodes in AEMFC [9,15]. More study of the effects of the uptake of CO_2 in the AEM is therefore important and necessary.

In this work, the effect of the presence of CO_2 and anions derived from its interaction with hydroxide is probed. Effects on the properties of a standard AEM membrane, A201, are studied. The membrane is examined in OH^-, HCO_3^-, and chloride (Cl^-) forms. The effects on the water uptake, density and conductivity, as well as the mobility of species in the water are studied. The conductivity of the AEM is determined at different water vapor activity levels. NMR spectroscopy is utilized to observe the water transport in the membrane by measuring the self-diffusion coefficient using PFG NMR techniques, also as a function of water content. ^{13}C NMR is used to characterize the HCO_3^- ion mobility in ^{13}C-labelled HCO_3^- form AEM. The diffusion coefficient of HCO_3^- ion thus obtained is used to calculate the conductivity using Nernst-Einstein (*N-E*) equation.

2. Experiment

2.1. Materials

A201 anion exchange membranes, provided in hydroxide form by Tokuyama Corporation, Japan, were used for all measurements in this study. Sodium hydroxide (1 M Certified), Potassium hydroxide (ACS grade), Lithium Chloride (ACS grade) and Sodium Chloride (ACS grade) were obtained from Fisher Scientific. ^{13}C labeled carbon dioxide with 99 atom% ^{13}C was purchased from Sigma-Aldrich packaged in a 1 L steel cylinder. 18 MΩ cm DI water was produced using a Milli-Q® water filtration system.

2.2. Membrane preparation

Membranes were exchanged from one ion form to another (e.g. OH^- to HCO_3^- form, OH^- to Cl^- form) by soaking the membrane in a 1 M solution of the desired sodium/potassium salt. Tokuyama A201 membrane was soaked in 1 N NaOH solution for 24 h to exchange to OH^- form, ensuring that any carbonate which formed under ambient conditions was removed and replaced with OH^-. The HCO_3^- form membranes were obtained by soaking the A201 membranes for 72 h in a 1 M KOH solution saturated with a large excess of CO_2 gas, while the Cl^- form membranes were prepared by immersing OH^- form membranes in 1 M NaCl solution for 72 h. The ion exchange procedures were completed at room temperature with one change of solution to ensure full anion exchange. Subsequently, the exchanged OH^- form and Cl^- form membranes were transferred to DI water for 24 h with at least 2 exchanges of solution to remove the excess salt, while the HCO_3^- form membranes were flushed with DI water to clean the membrane surface. All OH^- form membrane preparation was conducted in a N_2 filled glove box to prevent CO_2 contamination, while the HCO_3^- form and Cl^- form membranes were prepared in the ambient atmosphere. The ^{13}C NMR characterization showed that the HCO_3^- form membrane prepared as above was fully in HCO_3^- form, with negligible CO_3^{2-} ions because no ^{13}C resonance was observed at 170 ppm, which is the expected resonance frequency of CO_3^{2-} ions. Compared to the long ^{13}C NMR time scale in the range of 75 μs ~0.2 s on a 300 MHz NMR [39], the possible exchange between the HCO_3^- and negligible CO_3^{2-} is comparably rapid and does not affect the chemical shift of $H^{13}CO_3^-$ or its diffusion coefficient measurement.

2.3. Water uptake

The water vapor activity was controlled with LiCl solutions of different concentrations [40]. The pretreated membranes were blotted dry with Kim-wipes, and then suspended over the LiCl solutions for two weeks until the water absorption of the membranes reached equilibrium at a given water vapor activity and temperature. After recording the mass of wet membranes (m_{equ}), the membranes were dried under vacuum at 90 °C for 48 h and the dry mass (m_{dry}) was recorded. The OH^- form membrane was converted to Cl^- form before drying to prevent degradation of the cationic groups during drying. The experiments for OH^- form water uptake were performed in N_2-filled glovebox. In the glovebox, CO_2 is monitored and is less than 20 ppm (the limit of detection of the meter). However it is likely to be much less than this since ultrapure nitrogen is used and the glovebox contains a CDX carbon dioxide absorbent, made by Two Little Fishies for aquariums. The carbon dioxide absorbent is made of a mix of sodium and calcium hydroxides with a color indicator to show when it is exhausted. It's found that the absorbent in the glovebox still looks pristine after 12 months, as shown in Fig. S1. For hydroxide-form membranes, water uptake measurements were carried out in a sealed bottle inside the glovebox and conductivity measurements were performed by suspending the membrane-loaded conductivity cell in a polypropylene bottle filled with N_2 gas. The water uptake of HCO_3^- form membrane was measured after the membranes were equilibrated in CO_2 filled environment; while the experiments for the other Cl^- form membranes were performed in an ambient environment. For the hydroxide and bicarbonate-form materials, transfers to equilibration or measurement cells were performed in the glovebox.

The ion exchange capacity (IEC) of 1.7 mmol g^{-1} is provided by Tokuyama [41]. The water uptake study was performed from 25 °C to 80 °C, and the water content λ was calculated using the following Equation (1).

$$\lambda = \frac{\frac{(m_{equ} - m_{dry})}{m_{dry}} * 1000}{M_{H_2O} \times IEC} = \frac{moles\ H_2O}{moles\ N^+} \quad (1)$$

2.4. Density

The density of membranes was measured using AccuPyc 1340

pyconometers, which accurately measures the volume sample using gas displacement methods. The membranes were quickly transferred, folded and filled into the 0.1 cm^3 sample cup after they reached the equilibrium at specific water activity and temperature. The helium gas is filled into chamber and rapidly fills pores of the sample until a certain pressure is reached, and then the gas is discharged into a second empty chamber allowing computation of sample volume. The density of sample was obtained by dividing the sample mass by the volume. To check the stability of water uptake during the density measurement, the mass of membranes was measured before and after the measurements. The water uptake is considered to be stable because the loss of water was less than 1% after the pyconometry measurements.

2.5. Conductivity

Each membrane sample was mounted into a four-point conductivity cell and suspended over LiCl solutions with controlled water activities in sealed polypropylene bottles. The temperature (25 °C to 80 °C) was controlled by placing the polypropylene bottles in an ESPEC environmental chamber. The polypropylene bottles were filled with N_2 gas, CO_2 gas and air for OH^- form, HCO_3^- form and Cl^- form membrane respectively. Membrane conductivity was determined using potentio-electrochemical impedance spectroscopy (PEIS) technique with a Bio-logic SP-200 potentiostat. The membrane resistance was measured by applying a sweep from 10^5 to 1 Hz and circle fitting the resultant Nyquist plot to determine the high frequency resistance. The width and thickness of the membrane were then measured and the conductivity determined with Equation (2):

$$\sigma = \frac{L}{R*T*W} \tag{2}$$

Where R is the high frequency resistance determined from the Nyquist plot, W and T are the average width and thickness and L is the distance between the two inner electrodes. The membrane resistance was monitored for several days after changing the temperature until a steady state value is obtained.

2.6. NMR diffusion

The membrane was equilibrated with a given water vapor activity by placing over a LiCl solution for 2 weeks and packed in a 5 mm NMR tube. To replace any water lost during sample packing, the NMR tube was placed in a polypropylene bottle containing a LiCl solution for 1 week to re-equilibrate the membrane. All NMR samples were sealed and maintained under constant water vapor activity. Self-diffusion coefficients of water and HCO_3^- ions were determined by PFG NMR spectrometry. All ^1H NMR diffusion measurements were performed on a Varian VNMRS 500 MHz spectrometer (operating at 499.715 MHz for ^1H frequency) with a broadband OneNMR probe using a DOSY bipolar pulse pair stimulated echo pulse sequence. The gradient strength of this spectrometer was 0–60 G/cm, which was incremented in 16 steps. Water diffusion measurements were performed on the OH^- form A201 membranes from 25 °C to 70 °C, while the HCO_3^- and Cl^- form membranes were characterized at 25 °C only. Since the natural abundance of ^{13}C is very low (1.07%), ^{13}C enriched CO_2 gas was used to make HCO_3^- solutions and prepare HCO_3^- form A201 samples to obtain a higher signal/noise ratio for NMR measurements. ^{13}C NMR (75.432 MHz) diffusion measurements were acquired on a 300 MHz (^1H frequency) spectrometer with a DOTY Z-gradient diffusion probe with gradient strength 0–1200 G/cm using a bipolar pulse spin echo sequence. The self-diffusion coefficient D was determined by fitting data according to Stejskal-Tanner equation [42] 3.

$$I = I_0 * e^{-D(\gamma g \delta)^2\left(\Delta - \frac{\delta}{3}\right)} \tag{3}$$

Where I is the relative signal strength, I_0 is the signal in absence of the field gradient, γ is gyromagnetic ratio of the studied nucleus, g is the gradient strength, δ is the gradient pulse duration and Δ is the diffusion delay.

3. Results and discussion

The water content λ, expressed as the number of water molecules per functional group, was determined for the A201 membrane in various forms. Fig. S2(a-h) shows the water uptake of OH^- form A201 membranes as a function of water vapor activity values, while the results for HCO_3^- and Cl^- form membranes are plotted in Fig. 1(a) and (b). As shown in Fig. S2(a), OH^- form A201 membranes have a water content roughly equal to 17.5 at water vapor activity $a_w = 1$, while λ decreases to 3 at $a_w = 0.13$, 25 °C. Fig. S2 (h) shows the water uptake of membranes equilibrated at $a_w = 1$ at different temperatures. The water content of the OH^- form membrane shows an increasing trend from 25 °C to 40 °C. However, it drops at higher temperature (50 °C to 80 °C). The highest water content value of OH^- form A201 is ~24.5 when the membrane has been equilibrated at $a_w = 1$ at 40 °C.

The general shape of the curve for water uptake by the three membrane forms as a function of activity is similar and indeed is similar to that previously reported for most ion exchange materials [43–45]. The water content data of HCO_3^- form A201 membranes is plotted in Fig. 1 (a). At room temperature (25 °C), the water content of HCO_3^- form membrane decreases from 11 at $a_w = 1$ to $a_w = 0.32$. When equilibrated at $a_w = 1$, 50 °C, the HCO_3^- form membrane has highest λ value of 17. As we observe in Fig. 1 (a), in the low water uptake range ($\lambda < 6$), the water uptake gradually decreases as the temperature is increased; however, at the higher water uptake range ($\lambda > 6$), the water uptake increases first and then drops down later as the temperature increases.

To explain this phenomenon, two opposing tendencies have to be considered, following arguments made in the context of PEM membranes [45–47]. On the one hand, ΔH_{hyd} dominates the hydration at low water vapor activity and is relatively insensitive to temperature, while ΔS_{hyd} term increases with the temperature at high water vapor activity due to the unfavorable polymer configurational entropy associated with swelling, resulting in a less favorable ΔG_{hyd} for high levels of membrane hydration at higher temperature [47]. On the other hand, as the temperature increases towards the T_g of membrane, the polymer is mechanically weaker and easier to swell, which favors the membrane hydration and micro-pores opening [2]. In another words, water primarily solvates the cationic sites and anions in the membrane at low a_w (around $a_w < 0.8$, $\lambda < 6$), where ΔG_{hyd} is the main factor that contributes to water uptake change with increasing temperature. In the high a_w range (around $a_w > 80\%$, $\lambda > 6$), where water primarily swells the polymer, water uptake by the membrane increases with temperature due to opening of micro-pores and formation of hydrated clusters [2,48]. Similar to HCO_3^- form A201, the water content of Cl^- form A201 membrane shows a rapid drop at high a_w range (0.85–1). The majority of the water absorption by Cl^- form membrane occurs at a_w higher than 0.85, while the plot shows a slower decrease of water uptake at $a_w < 0.85$ as the a_w decreases. Also, the Cl^- form A201, with maximum λ value of 15, exhibits a smaller water uptake than OH^- form membrane. The water uptake of three membrane forms at 25 °C and 80 °C are compared in Fig. 1(c) and (d) respectively. Generally, the order of water uptake is $\lambda_{OH^-} > \lambda_{HCO_3^-} > \lambda_{Cl^-}$, which agrees with some previous reports for a model poly (arylene ether) AEM [49] and an PFAEM-Gen2 membrane made up of 3 M precursor with a PTFE backbone [50].

Though the shape of the sorption curve is generic and appears similar for both anion and cation exchange materials, we think it is important to point out that the underlying physical driving forces for this shape, especially at low water activity, are likely different for anionic and cationic membranes. In the latter, the sulfonate and proton are strongly hydrated; in the former, it is unlikely that the cationic fixed site

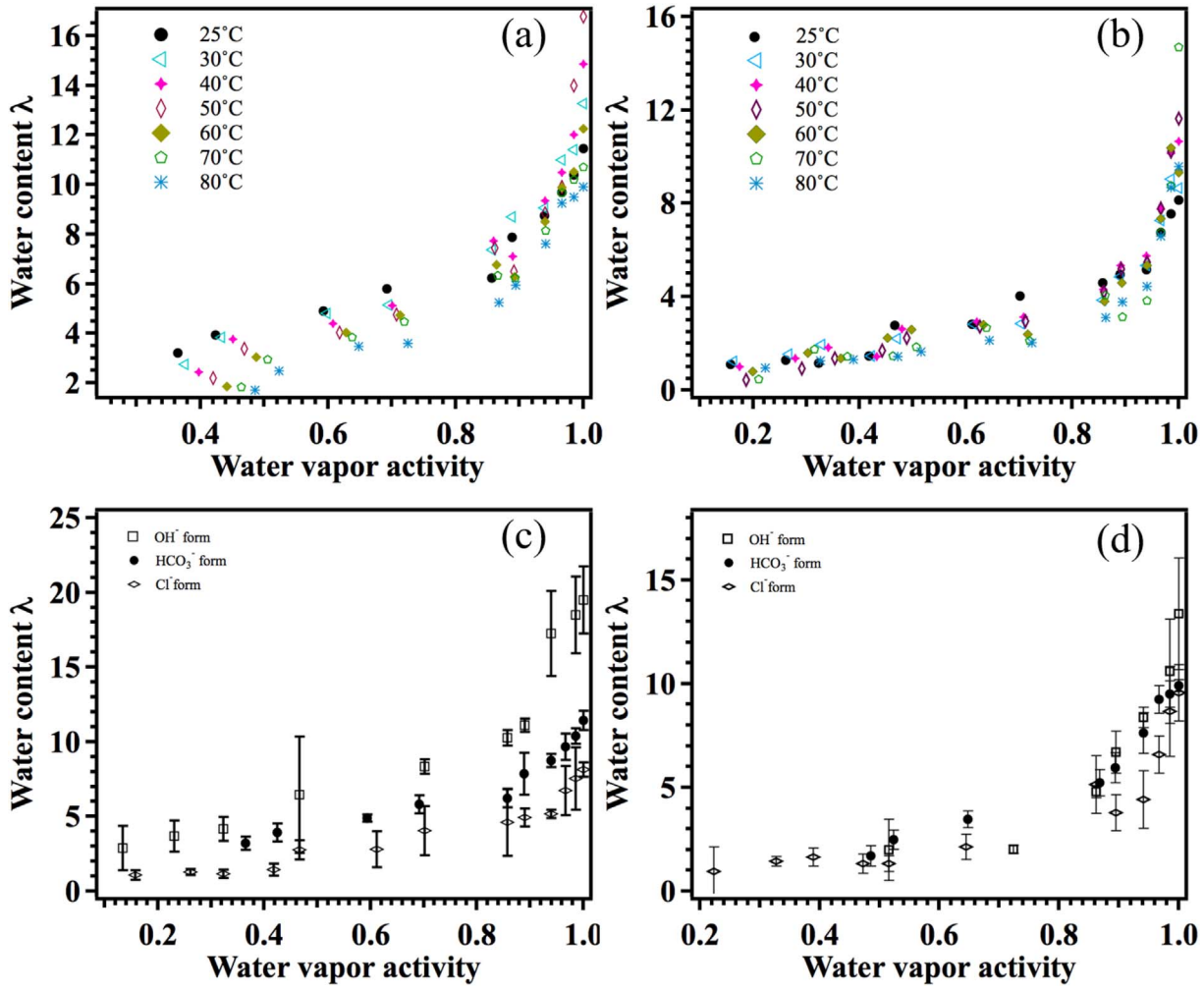

Fig. 1. The water uptake of HCO_3^- form (a) and Cl^- form (b) Tokuyama A201 membrane as a function of water vapor activity at 25 °C to 80 °C; the water uptake of three forms of Tokuyama A201 membrane as a function of water vapor activity at 25 °C (c) and 80 °C (d).

is strongly hydrated. This is perhaps reflected in the change in hydration at low activity with temperature. Thus, for the AEM, we expect the anion hydration enthalpy to be of primary importance.

To aid in further consideration of the processes occurring, Table 1 shows the Gibbs free energy of hydration in water and ionic radius of three anions studied in this work [51,52]. The order of the Gibbs free energy is ΔG_{hyd} (Cl^-) ≥ ΔG_{hyd} (HCO_3^-) > ΔG_{hyd} (OH^-), suggesting the HCO_3^- ions are slightly more hydrated than Cl^- ions, but less hydrated than OH^- ions, which agrees with our water uptake results shown in Fig. 1(c) and (d). (As a reminder to the reader, the free energies are negative so the largest free energy indicates the weakest interaction.) By comparing the Stokes radii of the ions, r (HCO_3^-) > r (OH^-) > r (Cl^-), indicating that the surface charge density (ρ_s) of the three ions should increase in the order ρ_s (HCO_3^-) < ρ_s (OH^-) < ρ_s (Cl^-). The surface charge density of the anion is not the only effect that contributes to ion hydration in this situation. Importantly, the strong hydrogen bonding interaction between anions (OH^- and HCO_3^-) and water facilitate the water solvation of these ions while Cl^- form membrane does not have this similar interaction. Therefore, the OH^- and HCO_3^- form membranes are expected to have a higher water content than that of Cl^- form membranes.

Density is an important parameter that is needed for calculating the molar concentration of functionalized groups and ions in ion exchange membranes. This is needed to calculate and interpret volume-based conductivity data [53] and is used below in discussion of the *N-E* equation in the hydrated polymer system. There are few literature reports of the density of PEMs, especially for hydrated samples. Nandan reported dry densities for a series of Nafion® 117 membranes in different ionic forms [54]. We reported the density of some PEMs as a function of water content [43]. However, we are not aware of any literature reports of the density of AEMs in the dry or hydrated state. We encountered difficulties in density measurements for OH^- form membrane because OH^- form membrane converts to HCO_3^- form rapidly by absorbing CO_2 upon exposure to air. Therefore, the density data were only collected on the HCO_3^- form and Cl^- form membranes. Fig. 2(a) shows the density of HCO_3^- form A201 membrane with different water content at various temperatures ranging from 25 °C to 80 °C. The density of hydrated HCO_3^- form membrane obtained at 25 °C and 80 °C varies between 1.10 g/cm^3 and 1.19 g/cm^3. For comparison, the density of hydrated perfluorinated membranes mentioned varies between 1.7 g/cm^3 to 2.5 g/cm^3, which is much higher than that of our AEM samples with hydrocarbon backbone. This difference is

Table 1
Ionic stokes Radius and Gibbs free energy of anions in water.

Anion species	r/nm	$\Delta_{hyd}G^*$/kJ mol^{-1}
OH^-	0.133	−430
HCO_3^-	0.156	−335
Cl^-	0.121	−317[a]/−340[b]

[a] Reported in Ref. [51].
[b] Reported in Ref. [52].

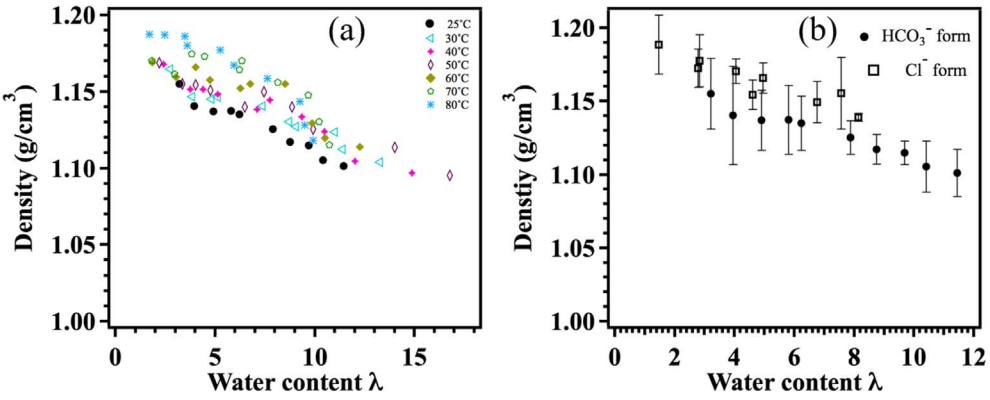

Fig. 2. (a) The density of HCO_3^- form Tokuyama A201 membrane as a function of water content at 25 °C to 80 °C; (b) The density of HCO_3^- and Cl^- form Tokuyama A201 membrane as a function of water content at 25 °C.

undoubtedly due to the fluorination of the PEMs. The membranes with highest water uptake (λ = 16.7) at 50 °C are the least dense and the membranes with lowest water uptake (λ = 0.5) at 80 °C are the most dense. The modest (8%) difference in density between the most hydrated and the driest membrane is understandable given the similarity of the dry polymer and water densities [43]. As the water content increases, the density of HCO_3^- form membrane decreases. The water molecules imbibed into the membrane swell the polymer and expand the volume of polymer structure. Moreover, adding the less dense water to the more dense polymer membrane also helps to lower the overall density of hydrated membrane. The density measurements were also performed on Cl^- form A201 after the membranes were equilibrated under different water activities at 25 °C. The plot in Fig. 2(b) shows the density of HCO_3^- form membrane is similar to that of the Cl^- form membrane at the same water content within experimental error.

Fig. 3(a–h) shows the ionic conductivity of the OH^- form AEM between 25 °C and 80 °C as a function of water content. The ionic conductivity of HCO_3^- and Cl^- form membrane is plotted in Fig. 4 (a) and (b) respectively. Generally, around λ > 6, the conductivity of HCO_3^- and Cl^- forms at different temperatures decrease slowly as the water content drops, while the conductivity of all three forms decreases much more rapidly with water content at low water uptake λ < 6. The ionic conductivity of the three membrane forms increases with the temperature. The conductivity of three different membranes at 25 °C and 80 °C are compared in Fig. 4(c) and (d), showing that σ (OH^-) > σ (Cl^-) > σ (HCO_3^-) in the high water content range. The maximum value of conductivity of the OH^- form varies from 0.026 S cm^{-1} at 25 °C to 0.132 S cm^{-1} at 80 °C. The HCO_3^- form membrane has a maximum conductivity between 0.014 S cm^{-1} at 25 °C and 0.031 S cm^{-1} at 80 °C. The results obtained from our conductivity measurements clearly indicate that the presence of CO_2 dramatically decreases the ionic conductivity of membrane, in agreement with previously reported results [55–57].

Adam et al. [55] reported a through-plane conductivity of 7.7 ± 0.8 mS cm^{-1} and 8.8 ± 0.6 mS cm^{-1} for CO_3^{2-} form and OH^- form poly(ethylene-co-tetrafluoroethylene)-derived radiation-grafted AEM at a_w = 1, 30 °C, respectively; Grew et al. [56] reported that the conductivity of OH^- form Tokuyama A201 drops dramatically after CO_2 was absorbed by equilibrating the membrane in the air; in addition, Kiss et al. [17] have reported the conductivity of SnowPure Excellion I-200 AEM in three different forms, which is in the order of $\sigma_{OH^-} > \sigma_{CO_3^{2-}} > \sigma_{HCO_3^-}$. Thus, qualitatively there is broad agreement that substituting carbonate or bicarbonate for hydroxide leads to significant decrease in conductivity. (We caution the reader that detailed quantitative comparisons may be difficult because of slightly different experimental approaches to controlling carbon dioxide.)

There are a number of possible causes of the observed changes. These include the inherent differences in mobility of the various anions due to ion size effects, the effect of the uptake of CO_2 on the water content in the membrane, the possibility of different hydration structures around the anion (e.g. the presence of significant H-bonding), access to 'structural' transport pathways and the relative tendency of each anion to form ion pairs with the cationic sites.

The conductivity of the HCO_3^- form membrane is slightly lower than that of Cl^- form membrane when compared at the same water uptake. This could be the result of the larger radius of HCO_3^- ions compared to Cl^- ions as described in Table 1, as well as a strong hydrogen bonding interaction between the HCO_3^- ion and water in the membrane. In aqueous solutions, the rank order of mobility values for these anions is consistent with our conductivity data in the membranes [58]. Unfortunately, this is still inconclusive in allowing us to sort the contributing factors discussed above. Interestingly, the mobility advantage of the OH^- form membrane largely disappeared in the low water content range. This is perhaps unsurprising in light of the possibility of extensive ion-pairing (or undissociated anions) under those conditions.

The PFG NMR technique measures the self-diffusion coefficient of different ionic species in the membrane system. It is especially useful for observing the high-abundance NMR active nuclei, such as ^1H. ^1H NMR diffusion coefficient measurements have been performed for OH^-, HCO_3^- and Cl^- form membranes with various hydration states at 25 °C. Because the hydrogen atoms exchange rapidly among water and OH^- groups in OH^- form membrane on the NMR time scales, there is only one ^1H resonance peak observed in OH^- form membrane system, as shown in Fig. 5 (a). Therefore, raw ^1H NMR water diffusion data on OH^- form membranes were fitted with a one-parameter decay, reflecting the indistinguishability of the water and OH^- ion self-diffusion coefficients in the membranes (Fig. 5(b)). (The D value thus obtained is a population-weighted average of the D values of each contributing species.) The ^1H self-diffusion coefficients in OH^-, HCO_3^- and Cl^- form membranes were plotted as a function of water content Fig. 5(c) and water vapor activity Fig. 5(d). The ^1H self-diffusion coefficients of these membranes decrease by 30–60-fold from the fully hydrated state to that with the lowest water uptake.

Water diffuses more rapidly in Cl^- form membrane than in OH^- and HCO_3^- form membranes. We infer that this is also related to the H-bonding interaction between anions (OH^- and HCO_3^-) and water which obstructs the transport of water in the membranes. By comparing the diffusion result at the same water vapor activity as shown in Fig. 5 (d), the ^1H diffusion coefficient of OH^- form membrane is higher than the other two forms. This is due to the higher water uptake of OH^- form membrane than the others while different membranes were equilibrated at same water vapor activity environment. This also reflects the high underlying mobility of hydroxide ion resulting from its transport via the structural (hopping) diffusion mechanism. A study of water transport of CO_3^{2-} form AEMs compared with Nafion® has been reported by Luo et al. [59]. The water diffusivity of a hexamethyl-*p*-terphenyl poly(dimethylbenzimidazolium) (HMT-PMBI), a commercial AEM, Fumapem®, and Nafion® were reported to be 4.9 × 10^{-10} m^2/s, 2.0 × 10^{-10} m^2/s and 3.8 × 10^{-10} m^2/s at a_w = 0.4 and 70 °C. Our

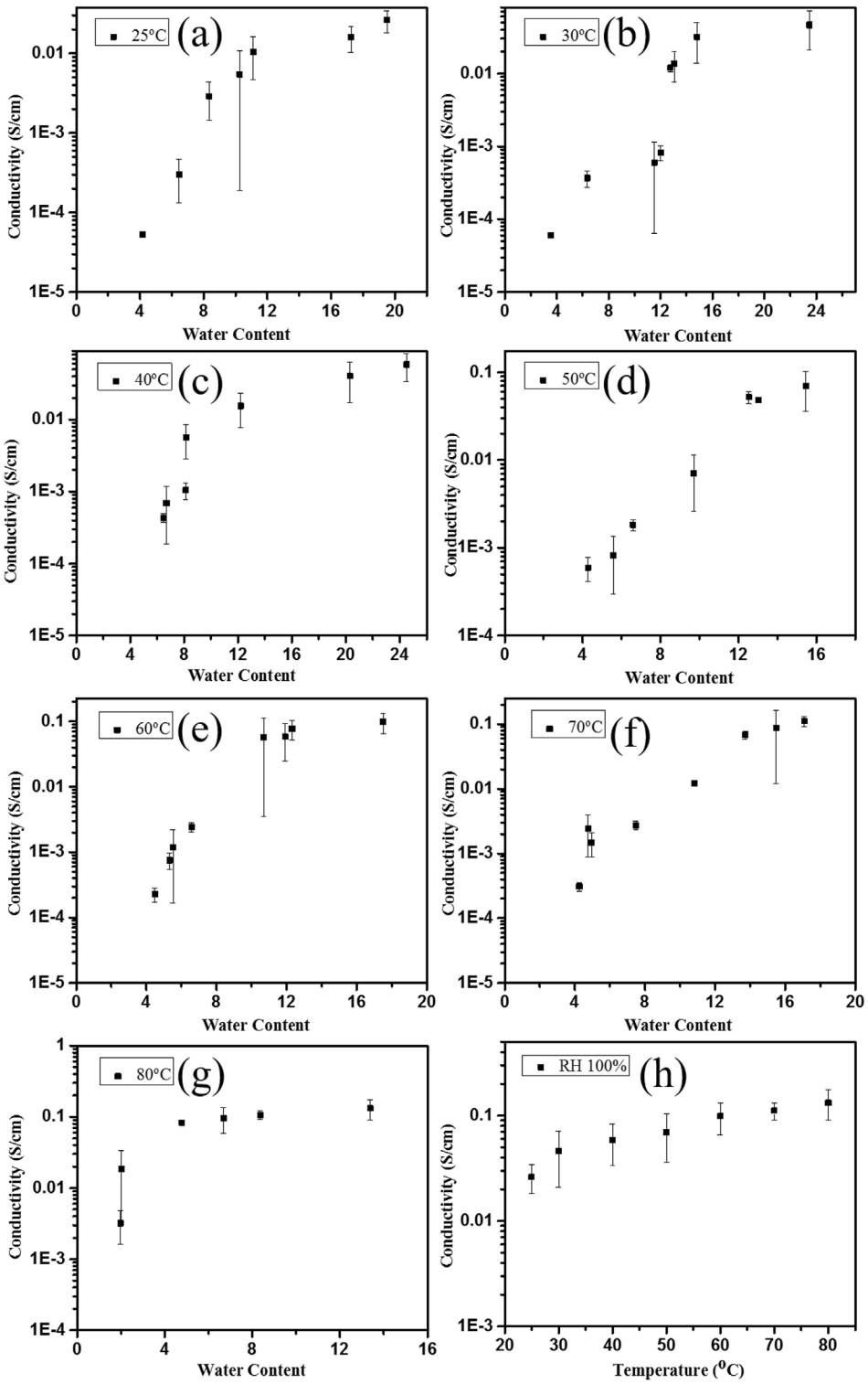

Fig. 3. Conductivity of OH^- form Tokuyama A201 as a function of water content λ at 25 °C to 80 °C, (a)–(g): 25 °C to 80 °C; (h) conductivity at water vapor activity $a_w = 1$.

data OH^- form Tokuyama A201 membrane at $a_w = 0.38$, 70 °C is 1.18×10^{-10} m^2/s, which is lower than values for these membranes. Moreover, an even lower D_{H_2O} is expected in HCO_3^- form Tokuyama A201.

The ^{1}H diffusion coefficients in OH^- form membranes were measured from 25 °C to 70 °C within the capability of our instrument, as shown in Fig. 6(a). The ^{1}H diffusion coefficients of OH^- form membrane equilibrated under water vapor ($a_w = 1$) is 6.8×10^{-10} m^2/s at 25 °C, then it increased to 1.7×10^{-9} m^2/s at 70 °C, which is about 2.5 times higher than the value at room temperature. The ^{1}H diffusion coefficient we obtained at 30 °C is 8.2×10^{-10} m^2/s, which is slightly higher than 7.4×10^{-10} m^2/s of the fully hydrated Nafion® 117 [45,60] and 7.6×10^{-10} m^2/s of 3 M PFSA PEM [61]. These values are within 10% of each other, a reasonable expectation of the experimental error, so interpretation may be moot. This result agrees with the water diffusion results obtained in PS-AEM and SDAPP PEMs reported by Hibbs et al. [19], who studied the diffusion coefficient of PS-AEM and SDAPP PEMs with different IEC. Generally, the water diffusion coefficient in AEMs increases with the IEC; moreover, the water diffusion coefficient of PS-AEMs is higher than that of SDAPP PEMs with similar IECs have

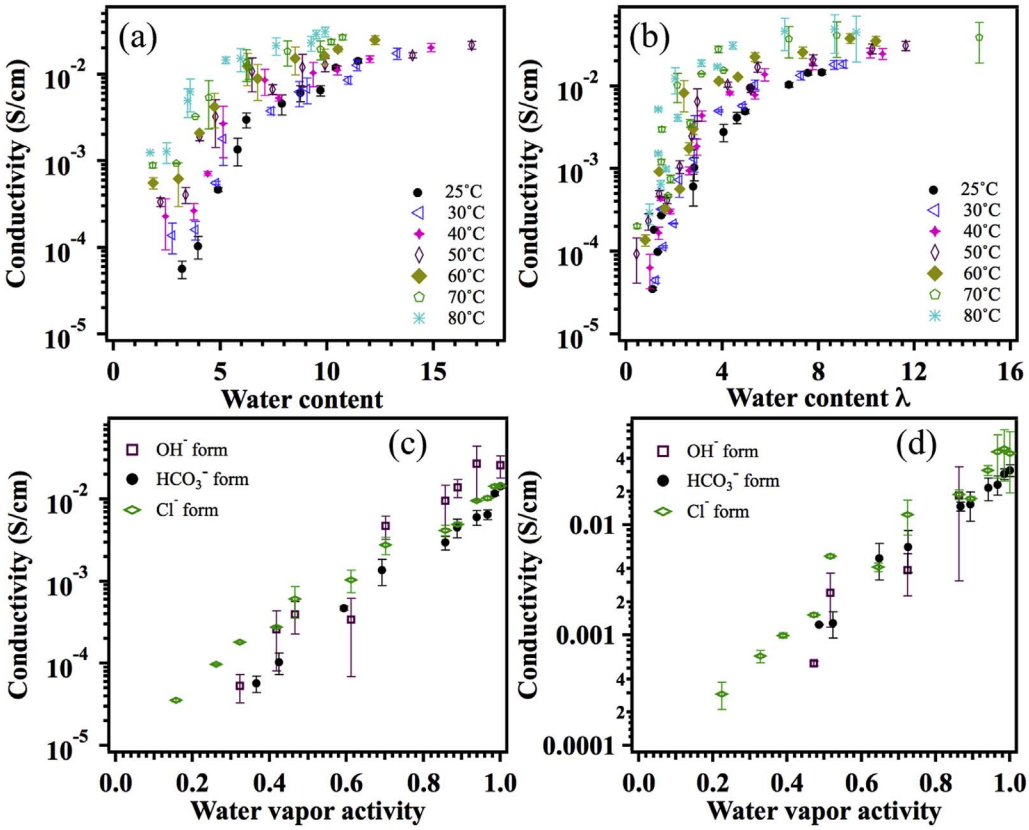

Fig. 4. Conductivity of Tokuyama A201 as a function of water content λ at 25 °C to 80 °C (a. HCO_3^- form; b. Cl^- form); the conductivity of three forms of Tokuyama A201 membrane as a function of water vapor activity at 25 °C (c) and 80 °C (d).

been equilibrated in liquid water. PS-AEMs, with IEC from 0.98 to 1.98 mmol g^{-1}, show a water diffusion coefficient in the range of 1.6×10^{-10} m^2/s to 7.6×10^{-10} m^2/s; while SDAPP PEMs with IEC of 0.91–2.2 mmol g^{-1} exhibit values of 9.9×10^{-11} m^2/s to 5.0×10^{-10} m^2/s. The Tokuyama A201 membrane we studied in this work, with IEC 1.7 mmol g^{-1}, show 5 times higher water diffusion

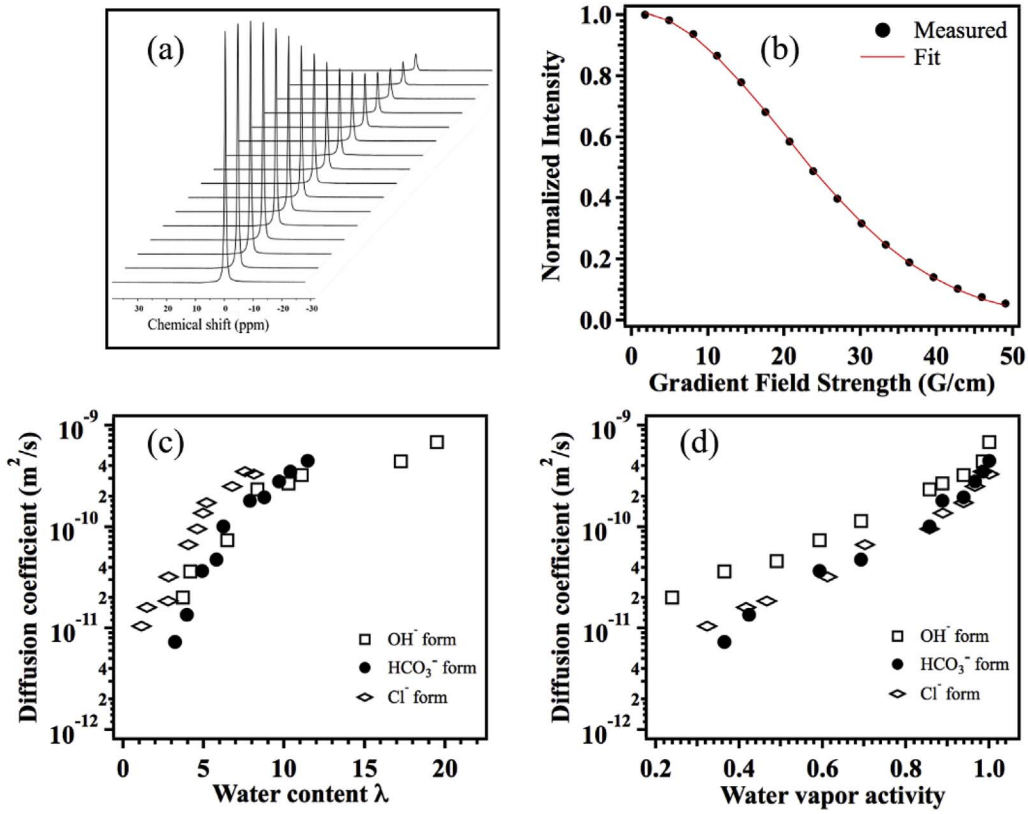

Fig. 5. (a) ^1H NMR spectra of PFG NMR experiments; (b) The fitting curve of diffusion coefficient using equation (3); Self-diffusion coefficient of water in OH^-, HCO_3^- and Cl^- form Tokuyama A201 as a function of (c) water content λ at 25 °C and (d) water vapor activity.

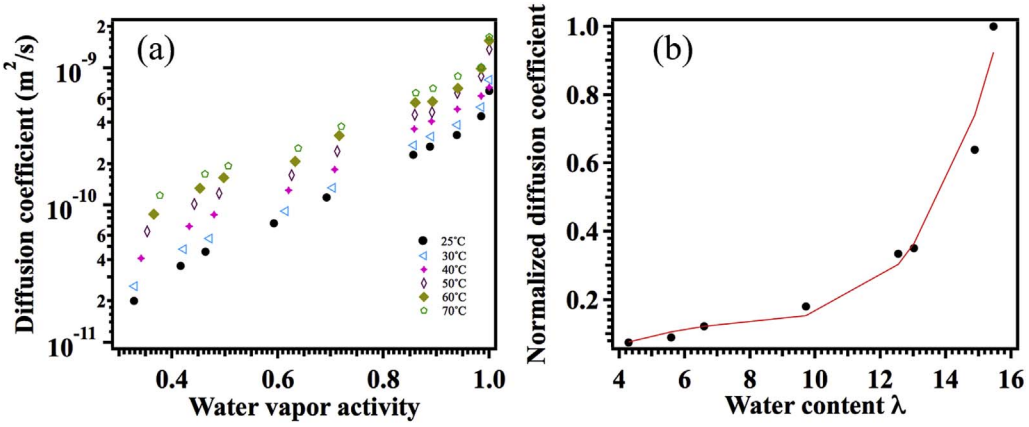

Fig. 6. (a) Self-diffusion coefficient of water in OH^- form Tokuyama A201 as a function of water vapor activity at 25 °C to 70 °C; (b) Normalized water diffusion coefficient in OH^- form membrane as a function of water content λ.

coefficient than PS-AEM with IEC 1.8 mmol g^{-1} at 25 °C [19].

The results in Fig. 6(a) indicate that the higher water content of OH^- form AEM and higher temperature support more rapid diffusion of water/OH^- ion. It is important to keep in mind what we probe in the NMR experiment. A typical diffusion time in the experiment is on the order of 100 ms. For the values of D typically observed, diffusion lengths will be roughly 5 to 10 μm. Thus, we can reasonably assume that the diffusing molecule samples all relevant local interactions as well the material tortuosity. Thus, polymers with different chemical functionality and morphology (typical channel or pore size, connectivity) will exhibit different water diffusivities. Disentangling these effects is beyond the scope of this paper for A201 and there is insufficient information available to do so for the other works cited.

Fig. 6(b) is a plot of normalized D as a function of OH^- form membrane water content λ. Springer et al. [62] have reported a simple polynomial fit to describe the correlation of D and water content λ in Nafion®. D was represented by a cubic polynomial for $\lambda > 4$ and by tabular interpolation for $\lambda \leq 4$ because D around $\lambda = 3$ is very sensitive to the variation of water activity [62]. Similarly, we include a fit that we hope will aid the use of this data in modeling studies. Here the diffusion coefficient of water is fit by a fourth order polynomial within the available D data we obtained in the region of $\lambda > 4$ as indicated in Equation (4). The diffusion coefficient of water in the membranes with $\lambda \approx 17$ were characterized at different temperatures from 25 °C to 70 °C and the data obtained was employed to calculate the activation energy using Equation (5). The fitting curve is shown in Fig. S6. The obtained activation energy 17.76 kJ/mol was applied in Equation (4). The parameters for each temperature have been listed in Table 2.

$$D = 10^{-6}\exp\left[17760\left(\frac{1}{303} - \frac{1}{273+T}\right)\right](A + B*\lambda + C*\lambda^2 + D*\lambda^3 + E*\lambda^4) \quad (4)$$

$$D = D_0 \exp\left(-\frac{E_a}{RT}\right) \quad (5)$$

The water in the membrane is the medium for anion transport. Therefore, we expect that the most crucial factor influencing the mobility of the ions is the water content of the membrane. ^{13}C NMR measurements were performed to characterize the bicarbonate anion self-diffusion coefficients at 25 °C. These are plotted as a function of water content in Fig. 7(a). The average self-diffusion coefficient of HCO_3^- ions was found to be 8.3×10^{-11} m^2/s at the highest water content ($\lambda = 11.4$) while it shows the lowest diffusion coefficient of 5.2×10^{-13} m^2/s at lowest water content ($\lambda = 3.2$).

Table 2
Polynomial fit parameters used at different temperatures.

T (°C)	A	B	C	D	E
25	−1710	−250	−4770	1490	−49.5
30	−9990	−49200	6420	−9.74	−4.11
40	10.5	115	756	−40.4	81.2
50	−153	−382	421	−61.3	2.74
60	−1000	−2550	991	−91.	2.73
70	147	−131	43.4	−4.38	14.4

While some of the aforementioned parameters (water uptake and conductivity) were measured for A201 under a more limited set of conditions [41], we also note that the authors of reference [41] did not control the anionic state of the polymer. It is reasonable to assume, in the absence of any comment in that work to the contrary, that care was not necessarily taken to avoid exposure of the membrane to air and thereby CO_2. Those authors interpreted the findings in terms of percolation aspects of the polymer. However, the validity of that interpretation is somewhat suspect since the description of a volume fraction-based percolation threshold in such a system presumes ideal mixing of water and polymer. This is clearly not the case: in Ref. [41] they show the volume of mixing and it is highly non-ideal. It is the chemical effect of providing sufficient water to promote dissociation of the anion from the cation site, not a percolation threshold, that defines the point at which conductivity increases sharply.

The anion diffusion coefficient can be related to conductivity through the *N-E* equation, given in Equation (6).

$$\sigma = \frac{CF^2}{RT} = (\nu_+ Z_+^2 D_+ + \nu_- Z_-^2 D_-) \quad (6)$$

Where C is the concentration of conductive ions, F is the Faraday constant, R is the gas constant, T is the thermodynamic temperatures, ν_+ and ν_- are the number of cations and anions per formula unit of electrolyte, Z_+ and Z_- are the valences of the ions, and D_+ and D_- are the diffusion coefficients of the ions. Here the only conductive ions are HCO_3^- ions, with ν_- and Z_- both equal to 1.

Some previous discussion has been devoted to the applicability of the *N-E* equation to reconcile the ion diffusivity and conductivity of different membranes. However, none of them reported that the calculated result corresponded to the measured conductivity. For example, Herring et al. [21] reported the conductivity value calculated using the *N-E* equation was significantly lower than the measured value in an AEM. Volkov et al. [63] claimed the opposite trend (*N-E* calculated value higher than measured) in a cation exchange membrane system. However, our analysis shows some interesting results which do not agree with either those conclusions above. Following our analysis reported elsewhere, HCO_3^- ion concentrations are expressed using two different methods. When the membrane ion concentration is expressed as molarity, the two common choices for system volume are that of the entire hydrated membrane (i.e., HCO_3^- form polymer + water) and the water imbibed in the membrane (i.e., excluding the volume of polymer and ions). In these cases, the concentration of HCO_3^- ions follow two different two expressions:

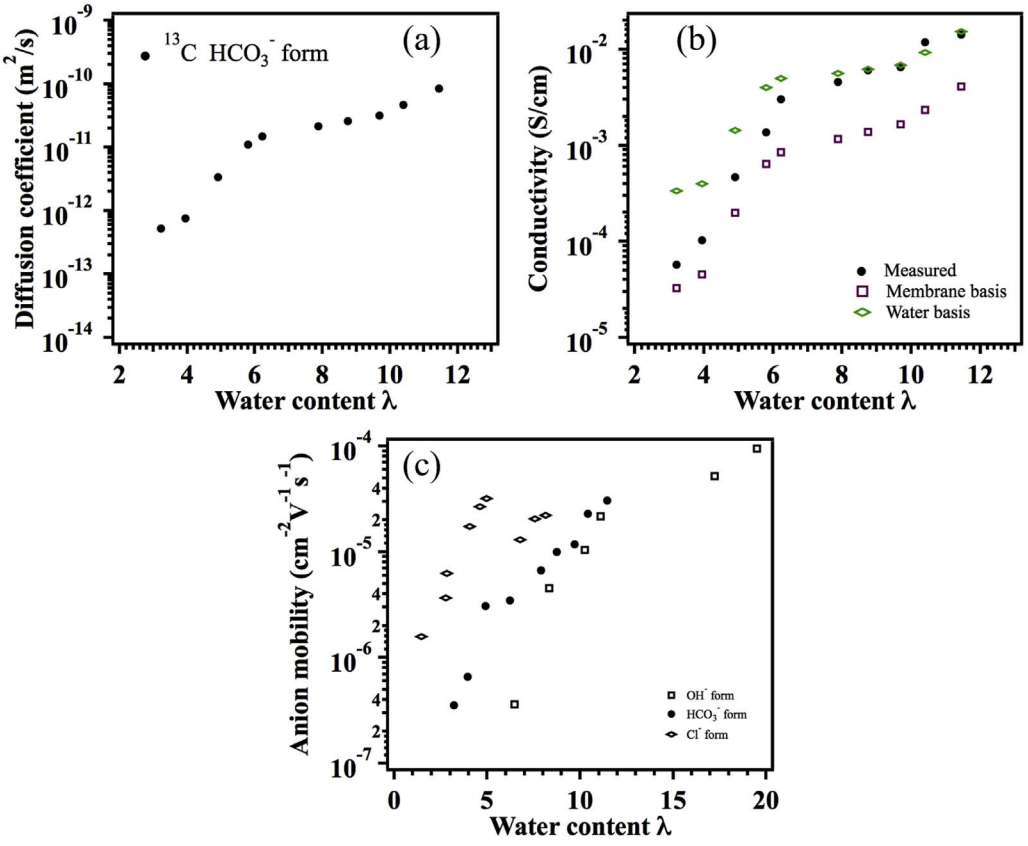

Fig. 7. (a) Self-diffusion coefficient of HCO_3^- ion in Tokuyama A201 as a function of water content λ at 25 °C; (b) the experimental conductivity data and calculated conductivity data using Nernst-Einstein equation as a function of water content at 25 °C; (c) The mobility data of anions in three different membrane forms.

Taking volume as volume of entire membrane:

$$C_{m+w} = \frac{1}{\left(\frac{MW_{membrane} + \lambda * MW(H2O)}{\rho_{(membrane+H_2O)}}\right)} \quad (7)$$

Taking volume as volume of absorbed water:

$$C_w = \frac{1}{\left(\frac{\lambda * MW(H2O)}{\rho_{H2O}}\right)} \quad (8)$$

Here $MW_{membrane} = 1000/IEC$ and $\rho_{(membrane+H_2O)}$ ($\rho_{(m+w)}$) was shown in Fig. 2(a) and (b).

The calculated conductivity from the two methods (Equations (6) and (7) or (6) and (8) compared to measured conductivity results are shown in Fig. 7(b). At higher water contents (about $\lambda > 6$), the σ_{m+w} were found to be very close to the $\sigma_{measured}$. As the water content increases, it appears that *N-E* equation applies if the concentration is calculated using water as the solvation media. Generally, the *N-E* equation was successfully applied using water as the ionic transport medium at higher water content. We attribute this to the highly hydrated ions moving through an environment which is similar to aqueous solutions. However, at lower water content, incompletely hydrated HCO_3^- ions move through or within a non-swollen membrane pore, perhaps between ionic sites, reflecting the bulk membrane nature.

The mobility of the anion can be calculated from conductivity data using Equation (9).

$$\sigma_{AEM} = Z_{anion^-} F C_{anion^-} u_{anion^-} \quad (9)$$

Where σ_{AEM} is the membrane conductivity; Z_{anion^-} is the valence of anion; F is the Faraday constant, 96500 C mol^{-1}; C_{anion^-} is the charge concentration, which will be defined in the following; and u_{anion^-} is the mobility of anion in the membrane.

Given the success of *N-E* equation for the HCO_3^- form AEM, the definition C_{anion^-} is also represented on a 'concentration in water' basis at high water content ($\lambda > 6$) and a 'concentration in membrane' basis at low water content ($\lambda < 6$). We note that λ around 6 was assumed as the demarcation point for two bases in the HCO_3^- form AEM system according to the discussion of Fig. 7(b). However, we are not able to similarly treat the OH^- form and Cl^- form AEM systems via the *N-E* equation because the diffusion coefficients of OH^- and Cl^- ions, and the density of OH^- form membrane were not readily measured. Therefore, we discuss the Cl^- mobility on the water basis at $\lambda > 6$ and on the membrane basis at $\lambda < 6$ based on assumed similar behavior; and OH^- mobility only on the water basis at $\lambda > 6$ since the membrane basis is not estimated because of the missing membrane density data. Fig. 7(c) shows the mobility of these three anions are in the order of $OH^- < HCO_3^- < Cl^-$ compared at the same water content, which is evidence that the hydrogen bond interaction is actually a hindrance for the OH^- and HCO_3^- transport in the membrane, particularly at lower water content. We also note that further consideration of the degree of dissociation of the anion-cation complex is warranted in this case. Indeed, one point of emphasis for our future work is a more thorough description of the hydration of both ions.

To summarize these findings, we present a schematic illustration of ion and water transport in AEM as shown Scheme 1. Generally, the mobility of anion and water are tied to the conductivity of the AEM, which is strongly affected by the interactions between functional group, anion and water molecules in the polymer. While the membrane is partially hydrated with low λ, the charged anion strongly bonds with quaternary ammonium functional group and there are mostly ion pairs in the polymer. As the water content increases, the water molecules promote the dissociation of anion and fixed catatonic group and yield more free ions in the polymer, thereby increase the conductivity of membrane. The size of anion also plays a role in determining the mobility of charge carrier. This is also one of the reasons that the HCO_3^- form membranes show smaller conductivity than OH^- form AEMs. The hydrogen bond network exiting between OH^- ions and H_2O molecules, and HCO_3^- ions and H_2O molecules facilitates the conductance of

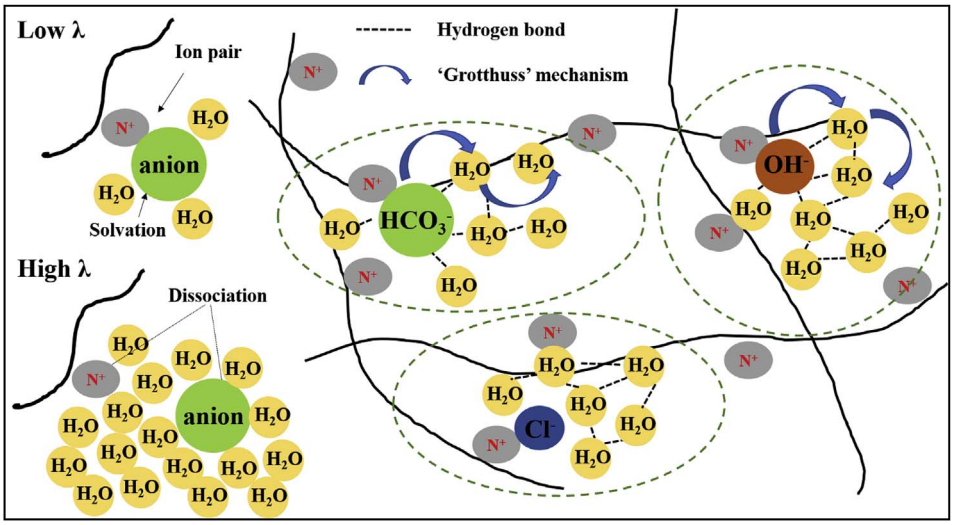

Scheme 1. The schematic illustration of ion and water transport in Tokuyama A201.

AEM, however, it also appears to hinder the water molecules to diffuse within the polymer. The OH^- ion and H_2O molecules form strong hydrogen bond networks and imbibe the highest λ in the AEM system. The hydrogen bond interaction facilitates the hopping of 'H' in the defect and promotes the conductance; however, it also hinders the transport of charge carrier and H_2O. For this reason, the transport of water in three different AEM systems show an opposite trend of hydrogen bond: $D_{H_2O}(Cl^-) > D_{H_2O}(HCO_3^-) > D_{H_2O}(OH^-)$ at the same (low) water content.

4. Conclusions

In this work, we studied and compared the water uptake, density, conductivity and ionic diffusivity of an anion exchange membrane Tokuyama A201 in the form of OH^-, HCO_3^- and Cl^-. The OH^- form membrane shows higher water uptake than the other two forms, indicating that a strong interaction exists between the OH^- ion and water molecules. The highest conductivity of OH^- form was 0.132 S cm^{-1} at 80 °C, which is about 3–4 times higher than the one of HCO_3^- form (0.031 S cm^{-1}) and Cl^- form (0.044 S cm^{-1}). The density of a hydrocarbon backbone AEM was measured for the first time, exhibiting apparent differences relative to a perfluorinated proton exchange membrane. The HCO_3^- form membrane and Cl^- form membrane show very similar density at the same water content. The diffusivity of the water in all three membrane systems was measured to evaluate the water transport properties. ^{13}C labeled HCO_3^- helps to distinguish the transport of charge carriers in AEM. By taking the concentration of charge carriers calculated using density data, the conductivity determined by ^{13}C NMR diffusion using the *N-E* theory successfully agreed with the measured conductivity values provided we take account of two situations occurring at different hydration levels.

Conflicts of interest

There are no conflicts to declare.

Acknowledgements

This work was funded by grants from the US Naval Research Office (N00014-16-1-2095 and N0014-16-1-2579). The authors thank Dr. Mallory Gobet of the Hunter College for discussion and support with the ^{13}C NMR diffusion measurements. The authors also thank Dr. Peter V. Bonnesen of Oak Ridge Laboratory for assistance with the ^{1}H diffusion NMR portion of this research, which was conducted at the Center for Nanophase Materials Sciences, which is a DOE Office of Science User Facility.

Appendix A. Supplementary data

Supplementary data related to this article can be found at http://dx.doi.org/10.1016/j.jpowsour.2018.01.071.

References

[1] M.A. Hickner, A.M. Herring, E.B. Coughlin, J. Polym. Sci. B Polym. Phys. 51 (2013) 1727–1735.
[2] G. Merle, M. Wessling, K. Nijmeijer, J. Membr. Sci. 377 (2011) 1–35.
[3] H.W. Zhang, D.Z. Chen, Y. Xianze, S.B. Yin, Fuel Cell. 15 (2015) 761–780.
[4] K. Matsuoka, Y. Iriyama, T. Abe, M. Matsuoka, Z. Ogumi, J. Power Sources 150 (2005) 27–31.
[5] L. Li, Y. Wang, J. Membr. Sci. 262 (2005) 1–4.
[6] J.-S. Park, S.-H. Park, S.-D. Yim, Y.-G. Yoon, W.-Y. Lee, C.-S. Kim, J. Power Sources 178 (2008) 620–626.
[7] T.P. Pandey, H.N. Sarode, Y. Yang, Y. Yang, K. Vezzù, V. Di Noto, S. Seifert, D.M. Knauss, M.W. Liberatore, A.M. Herring, J. Electrochem. Soc. 163 (2016) H513–H520.
[8] V. Ramani, Electrochemistry 14 (2017) 23.
[9] M. Inaba, Y. Matsui, M. Saito, A. Tasaka, K. Fukuta, S. Watanabe, H. Yanagi, Electrochemistry 79 (2011) 322–325.
[10] K.-D. Kreuer, P. Jannasch, J. Power Sources 375 (2017) 361–366.
[11] J.R. Varcoe, P. Atanassov, D.R. Dekel, A.M. Herring, M.A. Hickner, P.A. Kohl, A.R. Kucernak, W.E. Mustain, K. Nijmeijer, K. Scott, T. Xu, L. Zhuang, Energy Environ. Sci. 7 (2014) 3135–3191.
[12] D.R. Dekel, J. Power Sources 375 (2017) 158–169.
[13] T. Omasta, L. Wang, X. Peng, C. Lewis, J. Varcoe, W. Mustain, J. Power Sources (2017) 205–213.
[14] S. Gottesfeld, D.R. Dekel, M. Page, C. Bae, Y. Yan, P. Zelenay, Y.S. Kim, J. Power Sources 375 (2017) 170–184.
[15] H. Yanagi, K. Fukuta, Econ. Transit. 16 (2008) 257–262.
[16] J.A. Vega, C. Chartier, W.E. Mustain, J. Power Sources 195 (2010) 7176–7180.
[17] A.M. Kiss, T.D. Myles, K.N. Grew, A.A. Peracchio, G.J. Nelson, W.K.S. Chiu, J. Electrochem. Soc. 160 (2013) F994–F999.
[18] T.M. Alam, M.R. Hibbs, Macromolecules 47 (2014) 1073–1084.
[19] M.R. Hibbs, M.A. Hickner, T.M. Alam, S.K. McIntyre, C.H. Fujimoto, C.J. Cornelius, Chem. Mater. 20 (2008) 2566–2573.
[20] V. Volkov, Y.M. Popkov, S. Timashev, D. Bessarabov, R. Sanderson, Z. Twardowski, J. Membr. Sci. 180 (2000) 1–13.
[21] H.N. Sarode, Y. Yang, A.R. Motz, Y. Li, D.M. Knauss, S. Seifert, A.M. Herring, J. Phys. Chem. C 121 (2017) 2035–2045.
[22] P. Choi, N.H. Jalani, R. Datta, J. Electrochem. Soc. 152 (2005) E123–E130.
[23] D. Marx, ChemPhysChem 7 (2006) 1848–1870.
[24] S.J. Paddison, R. Paul, Phys. Chem. Chem. Phys. 4 (2002) 1158–1163.
[25] M.E. Tuckerman, D. Marx, M. Parrinello, Nature 417 (2002) 925–929.
[26] P. Vanysek, CRC Handbook of Chemistry and Physics, vol. 83, (2000).
[27] D.J. Pickett, Electrochemical Reactor Design, Elsevier Scientific Pub. Co, 1977.
[28] J.R. Varcoe, Phys. Chem. Chem. Phys. 9 (2007) 1479–1486.
[29] K.N. Grew, W.K. Chiu, J. Electrochem. Soc. 157 (2010) B327–B337.
[30] M. Tuckerman, K. Laasonen, M. Sprik, M. Parrinello, J. Phys. Chem. 99 (1995) 5749–5752.
[31] M.E. Tuckerman, K. Laasonen, M. Sprik, M. Parrinello, J. Phys. Condens. Matter 6 (1994) A93.
[32] J.R. Varcoe, R.C. Slade, Fuel Cell. 5 (2005) 187–200.
[33] T.P. Pandey, A.M. Maes, H.N. Sarode, B.D. Peters, S. Lavina, K. Vezzù, Y. Yang, S.D. Poynton, J.R. Varcoe, S. Seifert, Phys. Chem. Chem. Phys. 17 (2015)

4367–4378.
[34] C.-C. Yang, Mater. Sci. Eng., B 131 (2006) 256–262.
[35] Y. Wang, G. Wang, G. Li, B. Huang, J. Pan, Q. Liu, J. Han, L. Xiao, J. Lu, L. Zhuang, Energy Environ. Sci. 8 (2015) 177–181.
[36] L. Wang, E. Magliocca, E.L. Cunningham, W.E. Mustain, S.D. Poynton, R. Escudero-Cid, M.M. Nasef, J. Ponce-González, R. Bance-Souahli, R.C. Slade, Green Chem. 19 (2017) 831–843.
[37] G. Li, Y. Wang, J. Pan, J. Han, Q. Liu, X. Li, P. Li, C. Chen, L. Xiao, J. Lu, L. Zhuang, Int. J. Hydrogen Energy 40 (2015) 6655–6660.
[38] J.A. Vega, C. Chartier, S. Smith, W.E. Mustain, Econ. Transit. 33 (2010) 1735–1749.
[39] R.G. Bryant, J Chem. Educ. 60 (1983) 933.
[40] H.F. Gibbard, G. Scatchar, J. Chem. Eng. Data 18 (1973) 293–298.
[41] Q.J. Duan, S.H. Ge, C.Y. Wang, J. Power Sources 243 (2013) 773–778.
[42] E.O. Stejskal, J.E. Tanner, J. Chem. Phys. 42 (1965) 288–292.
[43] Y. Bai, M.S. Schaberg, S.J. Hamrock, Z. Tang, G. Goenaga, A.B. Papandrew, T.A. Zawodzinski Jr., Electrochim. Acta 242 (2017) 307–314.
[44] T. Kalapos, B. Decker, H. Every, H. Ghassemi, T. Zawodzinski, J. Power Sources 172 (2007) 14–19.
[45] T.A. Zawodzinski, C. Derouin, S. Radzinski, R.J. Sherman, V.T. Smith, T.E. Springer, S. Gottesfeld, J. Electrochem. Soc. 140 (1993) 1041–1047.
[46] J.T. Hinatsu, M. Mizuhata, H. Takenaka, J. Electrochem. Soc. 141 (1994) 1493–1498.
[47] P. Futerko, I.M. Hsing, J. Electrochem. Soc. 146 (1999) 2049–2053.
[48] Y.S. Li, T.S. Zhao, W.W. Yang, Int. J. Hydrogen Energy 35 (2010) 5656–5665.
[49] M. Marino, J. Melchior, A. Wohlfarth, K. Kreuer, J. Membr. Sci. 464 (2014) 61–71.
[50] A.G. Divekar, A.M. Park, Z.R. Owczarczyk, S. Seifert, B.S. Pivovar, A.M. Herring, Econ. Transit. 80 (2017) 1005–1011.
[51] Y. Marcus, J. Chem. Soc., Faraday Trans. 87 (1991) 2995–2999.
[52] T. Sata, Y. Yamane, K. Matsusaki, J. Polym. Sci. Polym. Chem. 36 (1998) 49–58.
[53] J. Daintith, A Dictionary of Chemistry, Oxford University Press, USA, New York, 2008.
[54] D. Nandan, H. Mohan, R. Iyer, J. Membr. Sci. 71 (1992) 69–80.
[55] L.A. Adams, S.D. Poynton, C. Tamain, R.C.T. Slade, J.R. Varcoe, Chemsuschem 1 (2008) 79–81.
[56] K.N. Grew, X. Ren, D. Chu, Electrochem. Solid State Lett. 14 (2011) B127–B131.
[57] A.M. Kiss, T.D. Myles, K.N. Grew, A.A. Peracchio, G.J. Nelson, W.K. Chiu, Econ. Transit. 50 (2013) 2175–2181.
[58] M.L. Disabb-Miller, Y. Zha, A.J. DeCarlo, M. Pawar, G.N. Tew, M.A. Hickner, Macromolecules 46 (2013) 9279–9287.
[59] X. Luo, S. Holdcroft, J. Power Sources 375 (2017) 442–451.
[60] T.A. Zawodzinski Jr., M. Neeman, L.O. Sillerud, S. Gottesfeld, J. Phys. Chem. 95 (1991) 6040–6044.
[61] M. Maalouf, C.N. Sun, B. Pyle, M. Emery, G.M. Haugen, S.J. Hamrock, T.A. Zawodzinski, Int. J. Hydrogen Energy 39 (2014) 2795–2800.
[62] T.E. Springer, T. Zawodzinski, S. Gottesfeld, J. Electrochem. Soc. 138 (1991) 2334–2342.
[63] V.I. Volkov, A.A. Pavlov, E.A. Sanginov, Solid State Ionics 188 (2011) 124–128.